Published online November 16, 2017

Special Section: Noninvasive Imaging of Processes in Natural Porous Media

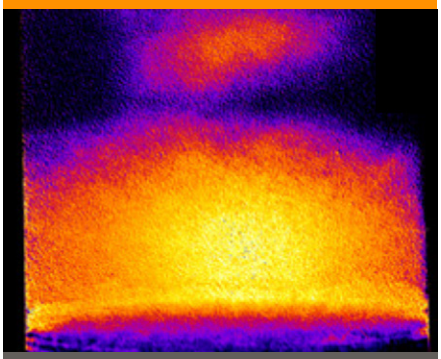

Core Ideas

- Water can be quantitatively detected in soil with X-ray radiography.
- We developed an easy calibration method to correct for beam hardening.
- We also eliminated drift of X-ray attenuation values due to detector latency.

Quantitative Analysis of Water Infiltration in Soil Cores Using X-Ray

Ulrich Weller,* Frederic Leuther, Steffen Schlüter, and Hans-Jörg Vogel

X-ray radiography is a suitable approach to study water dynamics in undisturbed soil. However, beam hardening impairs the deduction of soil moisture changes from X-ray attenuation, especially when studying infiltration of water into cylindrical soil columns. We developed a calibration protocol to correct for beam hardening effects that enables the quantitative determination of changing average water content in two-dimensional projections. The method works for a broad range of materials and is easy to implement. Moreover, we studied the drift of X-ray attenuation values due to the detector latency and eliminated its contribution to the quantitative analysis. Finally we could visualize the dynamics of infiltrating water into undisturbed cylindrical soil samples.

Abbreviations: CT, computed tomography.

Knowledge about the patterns of infiltration fronts in soil is important for a better understanding of the translocation of nutrients and pollutants (Hendrickx and Flury, 2001; Jarvis, 2007). However, direct, nondestructive observation of infiltration fronts in opaque soil is difficult. The visualization of water dynamics is important for a substantial understanding of many processes, such as water storage and solute transport. X-ray radiography and tomography can be used to determine differences in material density, and as such it is useful not only to investigate soil structure (Wildenschild and Sheppard, 2013) but also to study changes in water content (Hainsworth and Aylmore, 1983). Unfortunately, the measurement signal is small because water has a much lower attenuation of X-ray than mineral soil materials. The signal can be increased by adding tracers (Mori et al., 1999; Luo et al., 2008); however, high concentrations of heavy salts need to be applied for substantial improvement. This may lead to structural damage of the soil. Another approach uses the differences in X-ray attenuation at different energy levels, under the assumption that water attenuation has a constant value in Hounsfield units for any energy (Rogasik et al., 1999).

Another difficulty results from beam hardening as a critical feature when using polychromatic X-ray sources. Each wavelength has a specific attenuation coefficient, and with increasing path length through a sample the spectrum of the ray is shifted toward shorter wavelengths with a lower interaction probability. This has a strong influence on the attenuation coefficient of water along the cross-section of the sample, especially if the soil samples are cylindrical, as is typical for experiments on minimally disturbed soil cores. For circular cross-sections, the range of path lengths through the sample and therefore the range of attenuation values is very large. This effect has been neglected in previous studies (e.g., Bayer et al., 2004) but needs to be accounted for if quantitative results on changing water contents are to be analyzed. This is why it has been stated in the past that X-ray cannot be used for quantification of water infiltration (Allaire et al., 2009). Some researchers have overcome this limitation by applying three-dimensional computed tomography (CT) reconstruction, where the elimination of the beam hardening is part of the reconstruction process (Mooney, 2002). For high-resolution CT images, it is now possible to determine the distribution of water in the coarse pore space (e.g., Tracy et al., 2015). This is limited to steady-state images and to very small sample volumes.

Dep. of Soil Physics, Helmholtz Centre for Environmental Research–UFZ, Theodor-Lieser Str. 4, 06120 Halle (Saale), Germany. Ulrich Weller and Frederic Leuther contributed equally to this work. *Corresponding author (ulrich.weller@ufz.de).

Received 21 Dec. 2016.
Accepted 22 May 2017.

Citation: Weller, U., F. Leuther, S. Schlüter, and H.J. Vogel. 2017. Quantitative analysis of water infiltration in soil cores using X-ray. Vadose Zone J. doi:10.2136/vzj2016.12.0136

Because X-ray attenuation by water is small, some researchers have shifted to the application of neutron radiography (Moradi et al., 2011; Snehota et al., 2015). Kaestner et al. (2016) gave an overview of the different methods applied. While neutron probing is an excellent tool for imaging water, the availability of neutron beam lines is limited.

In the past, X-ray studies of water infiltration were mainly performed using flat, quasi-two-dimensional Hele–Shaw cells to minimize beam hardening effects and to homogenize the attenuation field. It is, however, close to impossible to obtain flat and rectangular soil samples that are only minimally disturbed, and the boundary effects of such samples are critical for flow and transport experiments. This is why flow and transport in soil is typically investigated in the laboratory using cylindrical samples (Allaire et al., 2009). Moreover, for cylindrical cores a sampling technology exists that minimizes structural disturbance (Kuka et al., 2013): a drill guided by a tripod cuts out the cylindrical shape, and short after the cutting blade a steel cylinder is guided over the soil column.

In this study, we developed a methodological approach to quantify water dynamics in terms of volumetric water content during transient infiltration experiments in cylindrical soil cores. It is based on a direct and sample-specific calibration procedure for the full range of soil and water content along the beam line through the circular cross-section of the cores.

Materials and Methods

Soil Samples

The approach was tested for 21 soil cores. In this study, we concentrated on three rather contrasting samples. They differed in soil material and in initial water content: two undisturbed soil samples with different textures (a sandy loam and a loamy sand according to FAO taxonomy) and a column filled with dry coarse sand. The sample cylinders were made of polycarbonate, with a wall thickness of 3 mm and an outer diameter of 100 mm. The sample heights were 100 mm for the undisturbed loamy sand and the coarse sand and 200 mm for the sandy loam. The loamy sand column was dried for 7 d in an oven at 50°C to reduce the initial water content, the sandy loam was at field moisture, and the coarse sand was oven dried at 105°C prior to the infiltration experiment. In this way, our approach could be tested for different situations ranging from a wet sandy loam where little change in moisture can be expected to a dry coarse sand with potentially strong gradients and sharp infiltration fronts. The soil textures of the different materials are given in Table 1.

Table 1. Grain size distribution for the studied materials.

Soil	Sand	Silt	Clay
	%		
Loamy sand	84	7	9
Sandy loam	65	16	19
Coarse sand	94	6	0

Experimental Design

The setup followed the multi-step flux configuration according to Weller and Vogel (2012). An irrigation device with 21 evenly distributed needles was installed on top of the samples to homogeneously spread the water on the entire surface. A constant water flux was provided by a peristaltic pump at a flux rate of $j = 8$ mm h^{-1}. For the coarse sand with its high hydraulic conductivity, we increased the flux rate to $j = 16.2$ mm h^{-1} after 168 min and to $j = 64.8$ mm h^{-1} after 242.5 min to detect further changes in water content. At the lower boundary, the cylindrical samples were covered with a perforated lid to stabilize the core and placed on a funnel-shaped support that was filled with saturated foamed clay pellets. Thus, percolating water drained freely (seepage boundary) and was transported to the outflow, where water was removed immediately using the same pump as for the irrigation system. To independently measure the total change in water content during infiltration, the entire experimental setup was mounted on a balance and the weight was automatically recorded every 20 s. The experiments were stopped when the total mass remained constant, assuming that an equilibrium of outflow and inflow was reached.

Radiography

The analysis was performed in an X-ray microtomograph (X-Tek XCT 225, Nikon Metrology) with classical radiography to monitor the two-dimensional projection of infiltrating water so that the shape and stability of wetting fronts were detected. To exploit the full range of gray values, slightly different energy settings were chosen for the different materials: loamy sand (140 keV, 470 μA), sandy loam (160 keV, 520 μA), and coarse sand (128 keV, 450 μA). To prevent overexposure at the lateral margins of the detector panel, we used a 2.0-mm (sandy loam), a 1.5-mm (loamy sand), and a 0.5-mm (coarse sand) copper filter. Radiographs were automatically taken every 150 s by averaging 16 frames with an exposure time of one frame per second. In between two records, the source of radiation was switched off to reduce gray value shifts due to latency of the panel.

The complete experimental setup was installed inside the X-ray chamber. To allow for calibrating the measured X-ray attenuation with respect to volumetric water content, the first image was made with an additional water column (radius 27 mm) installed horizontally behind the vertical soil core, which was relatively dry (see Fig. 1). Due to the cylindrical forms of the sample and the water column, this image provides (i) a water gradient in the vertical direction across the diameter of the water column and (ii) a gradient in soil thickness in the horizontal direction across the diameter of the soil sample. Afterward, the water column was removed and an image of the dry sample was taken. The sample was not moved during the entire experiment, which is critical for the following analysis.

A drawback of X-ray radiography is slight drifts in gray values due to charging or discharging of the panel while recording the images. The effect of latency varies in time and space because it is highly sensitive to the absorption of radiation from the penetrated material and to the history of the previous images. To reduce the influence of gray value shifts during the experiment, we preradiated the panel without the sample for 15 min using the same energy settings as for the subsequent experiment. Thus, the imaging started with a fully charged panel and the gray value drifts were limited to discharging processes. To detect the gray value drift, we installed two flat copper disks of different thicknesses close to the sample cylinder. The thicknesses of the disks were chosen such that their X-ray attenuation corresponded approximately to the minimum and maximum attenuation caused by the soil core (Fig. 1b). For the loamy sand, we used 1.5- and 11-mm-thick copper disks and 2.0- and 14-mm-thick disks for the sandy loam.

Image Analysis

The calibration procedure was based on the radiography of the soil columns at initial moisture content in combination with the water column (Fig. 1). This setup produced a broad range of well-defined water contents above the initial moisture according to the beam length within soil and water. For each pixel of the radiography, the X-ray beam has passed known lengths through soil and through additional water. This can be used for calibration. All image processing was done using the open source software packages QtQuantIm (Weller, 2010) and Fiji ImageJ V. 1.50d (Schindelin et al., 2012) in four steps.

Image generation (QtQuantIm)

A cylindrical projection for both the water column and the soil column was calculated. Additionally, the radiography of the dry soil with the water column was divided by the dry soil without the water column to obtain the attenuation due to the water column (water attenuation image c). Here, *dry* means the initial soil moisture of the sample before the irrigation had started.

Fitting (Gnuplot)

An automatic, randomized point data sampling of 300,000 pixels within the area of the projected water column was performed. For each pixel, the projected length of the water column (w), the initial gray value due to the soil column (s_0), and the value of the water attenuation image (c) was obtained. This gives the attenuation curve for the amount of water, where the attenuation coefficient is dependent on the initial attenuation by the soil column. The fit was based on minimizing the sum of squared residuals of the hyperbola exponential function and the sampled data by varying h_1, h_2, and h_3:

$$c = \exp\left[w\left(\frac{h_1}{s_0 + h_2} + h_3\right)\right] \quad [1]$$

Equation [1] needs fewer parameters and had a lower sum of errors of all the tested curves (exponential, polynomial, and rational).

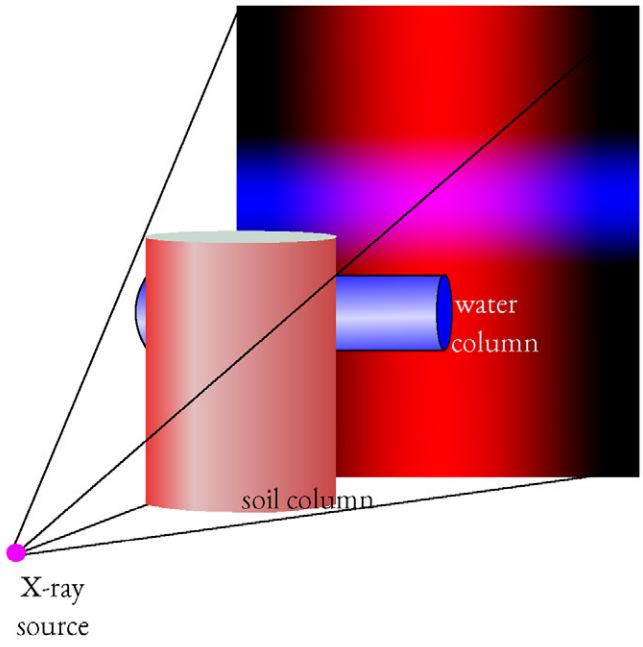

(a) Schematic set-up

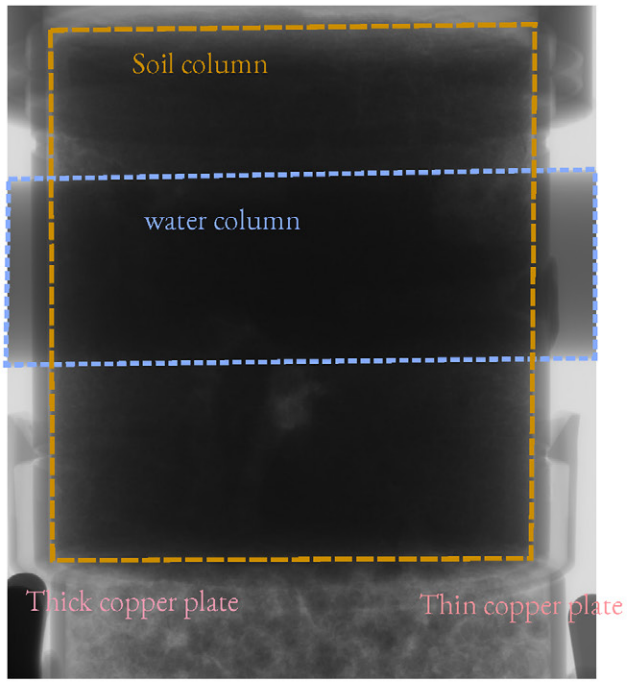

(b) Radiography

Fig. 1. Calibration setup with water column added.

Image Correction (Fiji)

To eliminate the effect of gray value drifts due to latency of the panel, we calculated the mean gray value for the thick (m) and thin (a) copper disks for every single time step (t) and corrected the initial gray values of the soil column (s_0) for the specific drift by assuming a linear relation between the drifts:

$$s_d = s_0 + \frac{s_0 - a_0}{m_0 - a_0}(m_t - m_0) + \left(1 - \frac{s_0 - a_0}{m_0 - a_0}\right)(a_t - a_0) \quad [2]$$

where m_0 and a_0 are the mean initial gray values, m_t and a_t are the mean gray values for the single time step (t), and s_d is the final gray value.

Water Quantification (QtQuantIm)

The amount of water (w_t) added during the experiment along the beam line was quantified in QtQuantIm for every single time step using

$$w_t = \frac{\ln\left(s_t / s_d\right)}{h_1/\left(s_d + h_2\right) + h_3} \quad [3]$$

where s_t is the gray value for the single time step, and s_d is the drift-corrected initial gray value.

Finally, the quantified water had to be translated into volumetric water content by dividing the result by the projection length of the soil column. For numerical reasons, the division image and the projection images were multiplied by an appropriate factor to use the full gray value range of a 16-bit image.

To check the accuracy of the method, water mass balance was calculated both by the mean volumetric water content across the entire soil sample calculated from the radiography and by the increase in total mass.

Results

Fitting

The relations between gray values of soil, water content, and their division is described by a hyperbola exponential function with three parameters: h_1, h_2, and h_3. Data points and the fitting curve of the loamy sand are plotted in Fig. 2; the color scheme of the single dots illustrates the individual vertical distance to the optimized curve. The method of sum of squared residuals provides a parameter fit for the different soils and moisture levels with an asymptotic standard error (ASE) not higher than 4% (Table 2).

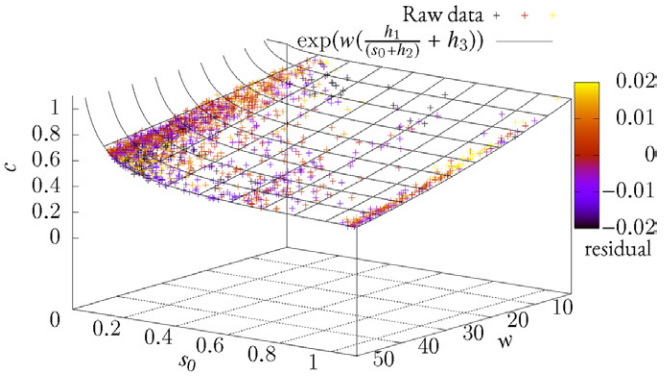

Fig. 2. Fitted hyperbola function for X-ray attenuation by water: attenuation due to added water column (c), initial attenuation by soil column (s_0), and the projected path length in the water column (w, mm).

Table 2. Fitting parameters for radiography evaluation for the three soil types.

Soil	h_1	h_2	h_3
Loamy sand	3.65×10^{-5} (1.6%)†	6.96×10^{-2} (3.8%)	-2.75×10^{-4} (0.1%)
Sandy loam	4.89×10^{-5} (1.0%)	8.89×10^{-2} (2.3%)	-2.64×10^{-4} (0.1%)
Coarse sand	3.45×10^{-5} (1.2%)	6.02×10^{-2} (2.7%)	-2.77×10^{-4} (0.1%)

† Asymptotic standard error in parentheses.

The fit for the sandy loam had the least maximum ASE of 2.3% for h_2. In comparison to the sandy loam and the coarse sand with a maximum error of 2.7% for h_2, the fit for the loamy sand has a higher instability, which results in a maximum error of 3.8%. The higher residuals of the single data points are evenly distributed across the entire range; therefore no systematic trend across the observed fitting range can be detected.

Applying the attenuation coefficient for water without correction for beam hardening in the dark parts, where the attenuation by soil is 0.1, would result in an underestimation of the water content. For the loamy sand and coarse sand only 25% and for sandy loam only 15% of the actual water would be detected.

Gray Value Drift

Figure 3 shows the mean gray value drifts with time of the 1.5- and 11.0-mm copper disks during n = 11 repetitions with the same experimental settings and their standard deviation. To start with a well defined latency, we pre-radiated the panel for 15 min to charge the panel. During the experiment, the radiation is absorbed by the material and therefore reduced in energy at the panel. This effect is enhanced by a discharging of the panel with time–the gray values are getting lower and therefore the drifts are negative. The thicker copper disks had a mean gray value of

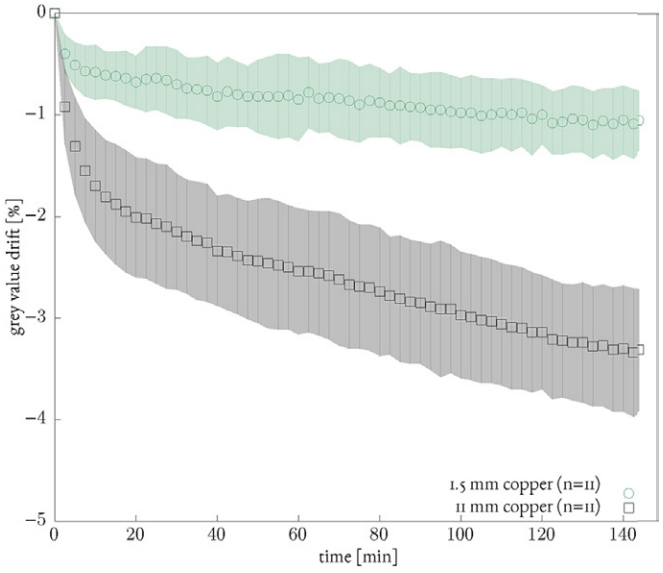

Fig. 3. Drift of the gray values due to panel latency.

around 4300, the thinner of 23,800. These values correspond to the brighter and darker areas in the image of the soil core. For the 11-mm copper disks, the mean gray values decrease by −3.5%, the 1.5-mm copper disks by −1.1%. The gray values of the soil are in between the gray value range of the copper disks and therefore are affected by the drift likewise. The data show a clear negative trend of the gray value drifts, which are related to the density of the radiated material. Hence, correction is necessary to prevent an overestimation of the water front because a negative drift would be interpreted as an increase in water content.

Infiltration Fronts via Two-Dimensional X-ray Radiography

Infiltration front propagation and the spatial moisture distribution of the different experiments are shown in Fig. 4.

Three images per sample from different time steps are presented from left to right for the loamy sand (A), the coarse sand (B), and the sandy loam (C). The images give the mean values of water content along the projected path length; local heterogeneities are pronounced in the lateral parts but are more leveled out in the

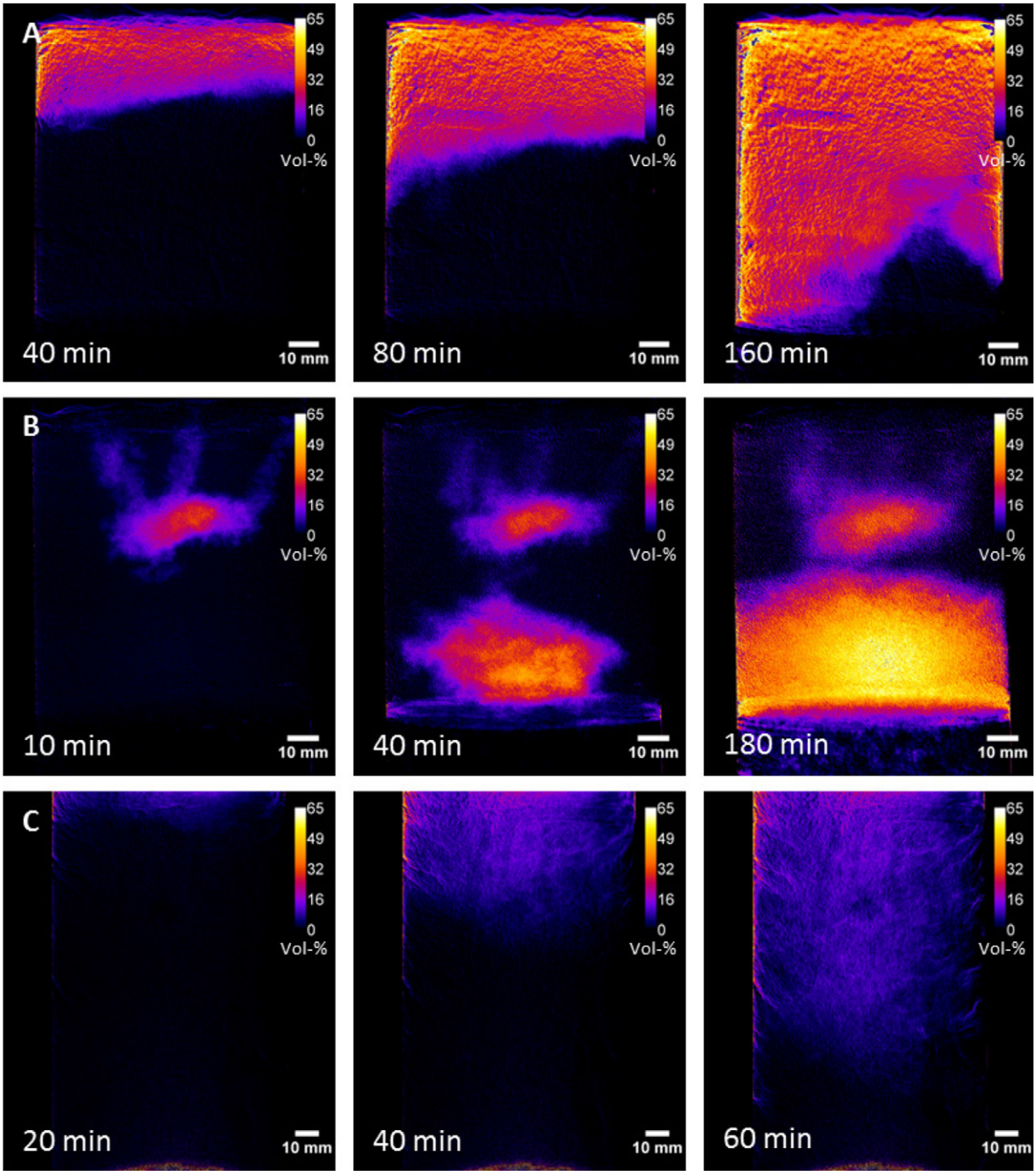

Fig. 4. Infiltration for three different soils: (A) loamy sand, (B) filled coarse sand, and (C) sandy loam.

central region. The color code illustrates changes in water content in a range from 65% (v/v); the values were calculated for every single pixel. Because the velocity of the infiltration front is primarily determined by the change in water content ($\Delta\theta$) across the infiltration front, this front passes much faster in the wet sandy loam than in the dry sandy soils. Therefore, different points in time are presented to better compare the spatial infiltration patterns for the different materials. The wetting front of the dried loamy sand is distributed across the entire sample width and proceeds homogeneously through the soil. The boundary between dry and completely wet soil is sharp. The final increase in water content for the entire sample was about 28.9% (v/v), while at the boundaries and in the uppermost part of the sample this increase was up to 55% (v/v) because here the soil was initially drier.

The coarse sand represents an excellent example of preferential flow in unsaturated, coarse-textured soils. Three narrow paths are sufficient to conduct the water to an artificial layer, where water accumulates before flowing to a second layer. In this experiment, the calculated change in water content is equal to the absolute water content because the filled coarse sand was oven dried. The paths on top and the one between the two layers have a mean water content of 7% (v/v), the upper water lenses up to 36% (v/v), and the lower up to 55% (v/v). The experiment shows high gradients in water contents and demonstrates the huge heterogeneity of the flow field in quantitative terms.

The total increase of soil moisture in the sandy loam was 5.6% (v/v); the infiltration front is clearly detectable for all time steps. Due to higher initial soil moisture in the column, the initial hydraulic conductivity ahead of the infiltration front is higher, the gradient in water content at the front is small (0–6% v/v), and therefore the front is less sharp. Because the clay minerals were already water saturated, artifacts of a swelling soil are negligible.

Quantification of Infiltrated Water

Figure 5 shows the change in water contents calculated by weight gain per volume and the mean determined gray value of the entire sample. The results demonstrate the applicability of the method but also a systematic overestimation of the water content. For the sandy loam the data are most reliable, with a maximum discrepancy of 1.9% (v/v) after 90 min. The coarse sand has a maximum discrepancy after 95 min (3.0% v/v), the loamy sand after 145 min (3.8% v/v). It was possible to detect the water dynamics in the sandy loam and the changes in water content due to increasing flux rates in the coarse sand after 168 and 242.5 min, respectively.

The consistency of the determined changes in water content were verified in a series of soil columns under two conditions (Fig. 6). The dried loamy sand had lower deviations and no drift with time, whereas the initially wetter sandy loam had up to 2% (v/v) mean drift.

Discussion

The differences in water content derived from radiography were in good agreement with the ones obtained via gravimetry. Also, the resulting images of water infiltration showed no lateral gradient due to the cylindrical shape of the soil column. Only at the very edge can an overestimation of water be assumed. Parts of the oversaturation at the boundaries are artifacts due to swelling processes of the soil into former air-filled areas. The method is based on density changes and cannot separate the radiation reduction due to increasing water content from that due to particle movement. The artifacts are therefore

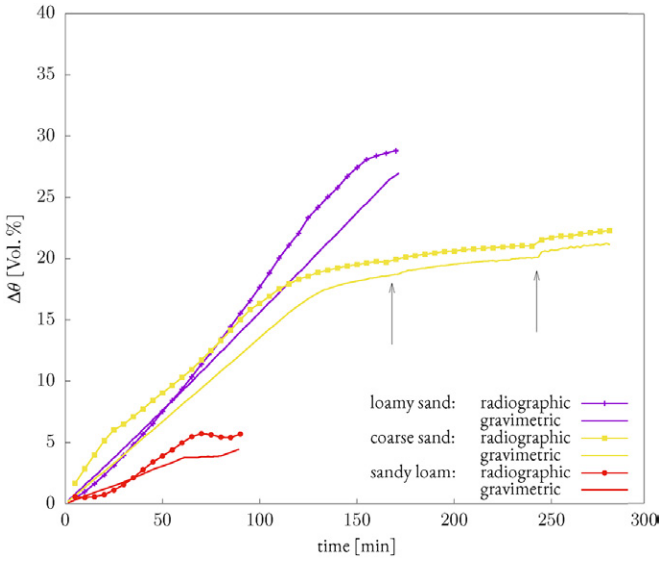

Fig. 5. Comparison of the change in water content ($\Delta\theta$) using gravimetric and radiographic methods for three different columns. Arrows indicate increasing flux rates.

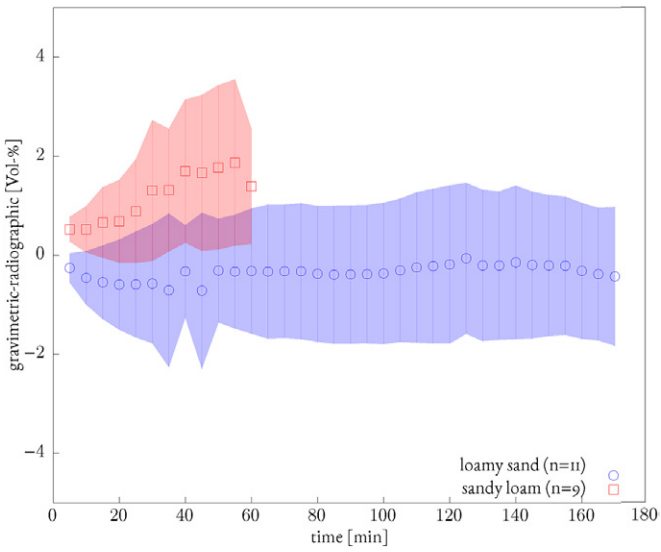

Fig. 6. Differences between radiometrically and gravimetrically determined changes in water content. Shaded areas indicate the standard deviation; boxes give the mean value for the replicates.

predominant at the edges where the radiated soil is thin and small changes have a strong impact on the mean gray value. Therefore, the first 10 pixel rows had to be excluded from further analysis. It can be assumed that the reconstruction of the water content is feasible and that beam hardening has been eliminated with the hyperbolic correction. However, there is no obvious explanation why the correction function should be a hyperbola. The calibration method allows the study of infiltration fronts in minimally disturbed soil columns, which is an advantage over cubic setups that have been studied previously based on radiography.

An obvious drawback of using radiography is the projection of the water content along the sample thickness such that details in the spatial patterns are blurred. This could be overcome with three-dimensional reconstruction of the water content. We did this experiment, calculating the water content for the whole set of 500 radiographs and recalculating the water contents into artificial attenuation images, which were then used for CT reconstruction using conventional filtered back-projection. The quality of the resulting images was, however, as noisy as direct CT reconstruction images and subsequent difference calculation of the Hounsfield values. The main disadvantage for the three-dimensional reconstruction remains: the series of radiographs has to be captured very fast if the water fronts are moving fast. In this case, the two-dimensional reconstruction is clearly superior.

Conclusions

With the presented procedure, it was possible to quantify changes in water content across the whole range of studied materials. We could eliminate the effects of beam hardening, which enabled us to use minimally disturbed, cylindrical soil cores for our infiltration studies.

This technique enables the visualization and quantification of fast-moving water fronts. It enables the quantitative study of heterogeneous water flow and of nonequilibrium dynamics with simple polychromatic X-ray radiography at a resolution that could be achieved before only by neutron probing or with monochromatic X-ray sources.

Acknowledgments

This work has been sponsored by the project "Impact of effluent irrigation on soil water dynamics and sustainable land use: Synergistic effects of altered soil structure and wettability (FKZ: 2813IL04)" of the German Federal Ministry of Food and Agriculture (BMEL). We thank our project partner Rony Wallach for coordinating the field campaign and Gil Lerner for his help during field work.

References

Allaire, S.E., S. Roulier, and A.J. Cessna. 2009. Quantifying preferential flow in soils: A review of different techniques. J. Hydrol. 378:179–204. doi:10.1016/j.jhydrol.2009.08.013

Bayer, A., H.-J. Vogel, and K. Roth. 2004. Direct measurement of the soil water retention curve using X-ray absorption. Hydrol. Earth Syst. Sci. 8:2–7. doi:10.5194/hess-8-2-2004

Hainsworth, J.M., and L.A. Aylmore. 1983. The use of computer-assisted tomography to determine spatial distribution of soil water content. Aust. J. Soil Res. 21:435–443. doi:10.1071/SR9830435

Hendrickx, J., and M. Flury. 2001. Uniform and preferential flow mechanisms in the vadose zone. In: Conceptual models of flow and transport in the fractured vadose zone. Natl. Acad. Press, Washington, DC. p. 149–187.

Jarvis, N.J. 2007. A review of non-equilibrium water flow and solute transport in soil macropores: Principles, controlling factors and consequences for water quality. Eur. J. Soil Sci. 58:523–546. doi:10.1111/j.1365-2389.2007.00915.x

Kaestner, A.P., P. Trtik, M. Zarebanadkouki, D. Kazantsev, M. Snehota, K.J. Dobson, and E.H. Lehmann. 2016. Recent developments in neutron imaging with applications for porous media research. Solid Earth 7:1281–1292. doi:10.5194/se-7-1281-2016

Kuka, K., B. Illerhaus, G. Fritsch, M. Joschko, H. Rogasik, M. Paschen, et al. 2013. A new method for the extraction of undisturbed soil samples for X-ray computed tomography. J. Nondestr. Test. 2013(8).

Luo, L., H. Lin, and P. Halleck. 2008. Quantifying soil structure and preferential flow in intact soil using X-ray computed tomography. Soil Sci. Soc. Am. J. 72:1058–1069. doi:10.2136/sssaj2007.0179

Mooney, S. 2002. Three-dimensional visualization and quantification of soil macroporosity and water flow patterns using computed tomography. Soil Use Manage. 18:142–151. doi:10.1111/j.1475-2743.2002.tb00232.x

Moradi, A.B., A. Carminati, D. Vetterlein, P. Vontobel, E. Lehmann, U. Weller, et al. 2011. Three-dimensional visualization and quantification of water content in the rhizosphere. New Phytologist 192:653–663. doi:10.1111/j.1469-8137.2011.03826.x

Mori, Y., T. Maruyama, and T. Mitsuno. 1999. Soft X-ray radiography of drainage patterns of structured soils. Soil Sci. Soc. Am. J. 63:733–740. doi:10.2136/sssaj1999.634733x

Rogasik, H., J.W. Crawford, O. Wendroth, I.M. Young, M. Joschko, and K. Ritz. 1999. Discrimination of soil phases by dual energy X-ray tomography. Soil Sci. Soc. Am. J. 63:741–751.

Schindelin, J., I. Arganda-Carreras, E. Frise, V. Kaynig, M. Longair, T. Pietzsch, et al. 2012. Fiji: An open-source platform for biological-image analysis. Nat. Methods 9:676–682. doi:10.1038/nmeth.2019

Snehota, M., V. Jelinkova, M. Sobotkova, J. Sacha, P. Vontobel, and J. Hovind. 2015. Water and entrapped air redistribution in heterogeneous sand sample: Quantitative neutron imaging of the process. Water Resour. Res. 51:1359–1371. doi:10.1002/2014WR015432

Tracy, S.R., K.R. Daly, C.J. Sturrock, N.M.J. Crout, S.J. Mooney, and T. Roose. 2015. Three-dimensional quantification of soil hydraulic properties using X-ray computed tomography and image-based modeling. Water Resour. Res. 51:1006–1022. doi:10.1002/2014WR016020

Weller, U. 2010. QtQuantIm users guide. Helmholtz Centre for Environmental Research–UFZ, Halle, Germany. www.quantim.ufz.de.

Weller, U., and H.-J. Vogel. 2012. Hydraulic conductivity and non-equilibrium across drainage and infiltration fronts. Vadose Zone J. 11(3). doi:10.2136/vzj2011.0134

Wildenschild, D., and A.P. Sheppard. 2013. X-ray imaging and analysis techniques for quantifying pore-scale structure and processes in subsurface porous medium systems. Adv. Water Resour. 51:217–246. doi:10.1016/j.advwatres.2012.07.018